

RESEARCH ARTICLE | FEBRUARY 21 2023

Bouncing droplets on micro-grooved non-wetting surfaces



Shi-Zheng Wang (王世正); Xianfu Huang (黄先富) ✉ ; Longquan Chen (陈龙泉) ;
Ying-Song Yu (余迎松) ✉



Physics of Fluids 35, 027118 (2023)

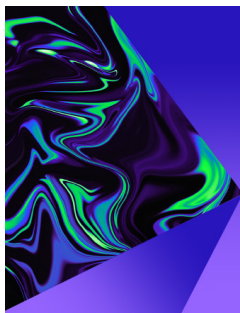
<https://doi.org/10.1063/5.0134783>



View
Online



Export
Citation



Physics of Fluids

Special Topic:

Selected Papers from the 2023 Non-Newtonian
Fluid Mechanics Symposium in China

Submit Today

Bouncing droplets on micro-grooved non-wetting surfaces

Cite as: Phys. Fluids **35**, 027118 (2023); doi: 10.1063/5.0134783

Submitted: 14 November 2022 · Accepted: 26 January 2023 ·

Published Online: 21 February 2023






View Online



Export Citation



CrossMark

Shi-Zheng Wang (王世正),¹ Xianfu Huang (黄先富),^{2,3,a)}  Longquan Chen (陈龙泉),^{4,5} 
and Ying-Song Yu (余迎松)^{1,6,a)} 

AFFILIATIONS

¹Department of Mechanics, School of Civil Engineering, Architecture and Environment, Hubei University of Technology, Wuhan 430068, People's Republic of China

²State Key Laboratory of Nonlinear Mechanics, Institute of Mechanics, Chinese Academy of Sciences, Beijing 100190, People's Republic of China

³School of Engineering Science, University of Chinese Academy of Sciences, Beijing 100049, People's Republic of China

⁴Yangtze Delta Region Institute (Huzhou), University of Electronic Science and Technology of China, Huzhou 313001, People's Republic of China

⁵School of Physics, University of Electronic Science and Technology of China, Chengdu 610054, People's Republic of China

⁶Innovation Demonstration Base of Ecological Environment Geotechnical and Ecological Restoration of Rivers and Lakes, Hubei University of Technology, Wuhan 430068, People's Republic of China

^{a)}Authors to whom correspondence should be addressed: huangxf@imech.ac.cn and yuys@hbut.edu.cn

ABSTRACT

Water droplets impinging on micro-grooved polydimethylsiloxane surfaces were studied. Depending on the impact velocity and surface roughness, different phenomena such as no bouncing, complete rebound (CR), bouncing occurring with droplet breakup (BDB), partial rebound, and sticky state were observed. The lower limit of impact velocity for bouncing droplets can be determined by balancing the kinetic energy of the droplet with energy barrier due to contact angle hysteresis. To predict the upper limit of impact velocity for bouncing droplets, a high-speed camera was used to record droplet impact at an ultrahigh speed and it was found that the transition from CR to BDB was attributed to a local wetting transition from the Cassie–Baxter state to the Wenzel state. Based on the experimental observation, a theoretical model was developed to predict the upper limit of impact velocity taking into account the penetration of the liquid into the micro-grooves. In addition, there was a shorter contact time of bouncing droplets with the decrease in the Weber number and surface roughness has a small influence on the contact time in our experiments.

Published under an exclusive license by AIP Publishing. <https://doi.org/10.1063/5.0134783>

I. INTRODUCTION

Micro-/nano-grooved surfaces usually exhibit a great anisotropy in surface wettability, which could be utilized for directional liquid transportation.^{1–5} Hence, such textured surfaces have found great applications such as water repellency,⁶ water harvesting,⁷ and condensation heat transfer enhancement.⁸ Meanwhile, droplet impinging on solid surfaces is ubiquitous in nature and the industry, and it has found great applications in agriculture and the industry.^{9,10} Therefore, an investigation of droplet impact on micro-grooved surfaces is of great significance.

When droplets are gently deposited on a micro-patterned surface, the droplets will be at one of the three wetting states, viz., the Wenzel wetting state¹¹ (liquid fully occupies the cavities between the

micro- and nano-structures), the Cassie–Baxter wetting state¹² (the droplet sits on the surface with the existence of an air cushion between the liquid and the bottom of the textured surface), and the mixed wetting state¹³ (some part of the surface is Wenzel-wetted while other part is Cassie–Baxter-wetted). Indeed, a pure Wenzel or Cassie–Baxter wetting state is a rare occurrence.^{14,15} The transition from the Cassie–Baxter wetting state to the Wenzel wetting state is available when an external pressure,^{16–18} vibration,¹⁹ or surface acoustic wave²⁰ is applied to the system. Recently, such a wetting transition has been also observed during the evaporation of sessile droplets on micro-patterned surfaces.^{21–24} Because the adhesion between the droplet and the micro-/nano-grooved surface behaves differently between along the longitudinal direction and along the transverse one (see Fig. 1),

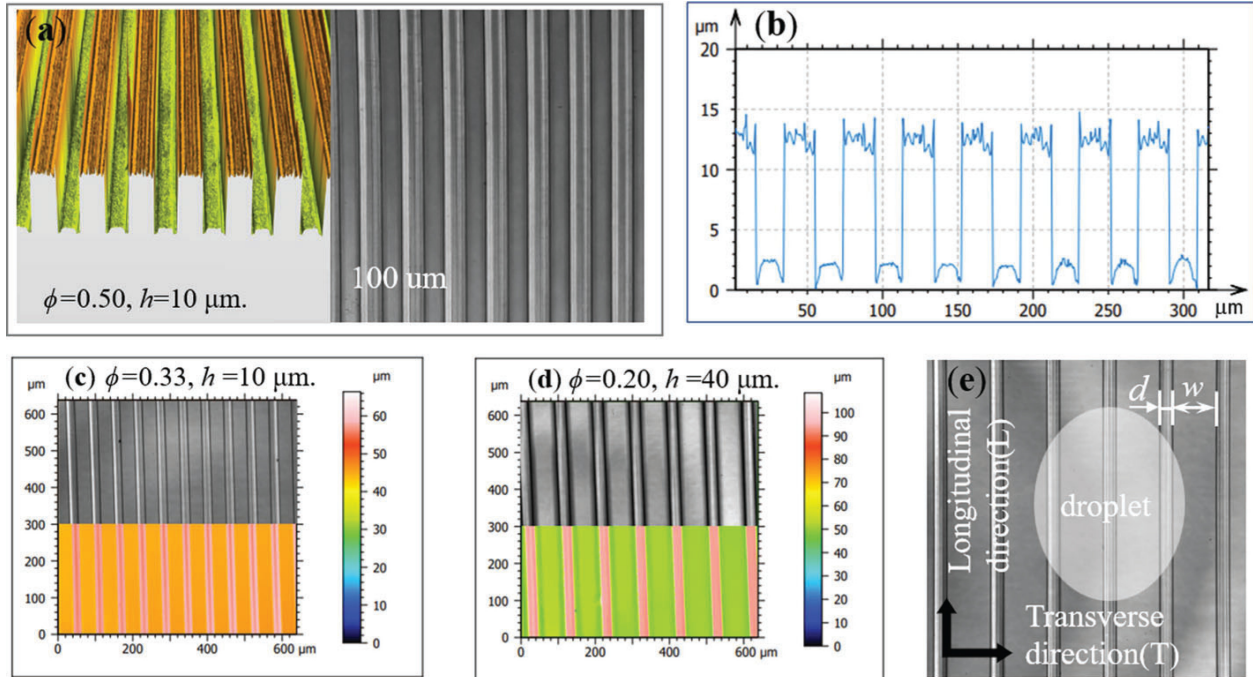


FIG. 1. Characterization of micro-grooved PDMS surfaces. (a) Top view of a micro-grooved PDMS surface, (b) LSCM characterization, (c) and (d) top view of micro-grooved PDMS surfaces, and (e) schematics of a droplet on a micro-grooved PDMS surface.

micro-/nano-grooved surfaces have different surface wettabilities depending on the shape of the stripe, the size of the stripe, the ratio of the stripe width to the stripe-to-stripe spacing, and the arrangement of stripes. Not only the static apparent contact angle but also the advancing and receding contact angles have different values along the two directions. Usually, the apparent, advancing, or receding contact angle along the transverse direction has a larger value than that along the longitudinal direction.

During the latest decades, droplet impact on rough surfaces including micro-/nano-pillar surfaces,^{25–29} hierarchical surfaces,³⁰ wrinkled surfaces,³¹ micro-grooved surfaces,^{32–40} and cylindrical ridges⁴¹ has been widely investigated and it was found that different impact phenomena including no bouncing (NB), complete rebound (CR), bouncing occurring with droplet breakup (BDB), partial rebound (PR), sticky state (SS), splashing as well as jetting, and bubbles will be observed depending on parameters such as impact velocity, surface wettability, physical and chemical properties of the liquid, substrate elasticity, and environmental condition.^{9,10} It has been widely accepted that the transition from CR to BDB/PR has been attributed to the wetting transition from the Cassie–Baxter state to the Wenzel state;^{26,27,32,42–46} however, there is still a lack of more detailed experimental observation. Moreover, predicting the lower and upper limits of impact velocity for bouncing droplets theoretically is of great importance. In addition, the contact time^{25,47–51} is also an important parameter for bouncing droplets. In the works by Wang *et al.*,^{26,27} it was found that for the case of micro-pillared polydimethylsiloxane (PDMS) surfaces, surface roughness greatly influences the contact time of bouncing droplets. As micro-grooved surfaces exhibit great anisotropy, how does the contact time of impinging droplets bouncing off these surfaces behave?

In this work, wettability of de-ionized water droplets on micro-grooved polydimethylsiloxane (PDMS) surfaces and de-ionized water droplets impinging on these surfaces are experimentally investigated. It was found that these surfaces have quite low wettability, but the effect of anisotropy is strong. The lower limit of impact velocity for bouncing droplets was theoretically analyzed by balancing the kinetic energy with energy barrier due to contact angle hysteresis. To elucidate the upper limit of impact velocity for bouncing droplets, penetration of the liquid into the cavities between the microstrips was experimentally observed using a high-speed camera. Then, a theoretical model was developed to predict the upper limit of impact velocity taking into account liquid penetration. Moreover, the contact time of bouncing droplets was analyzed and it was found that surface roughness has a small influence on the contact time.

II. MATERIALS AND METHODS

A. Substrate preparation

Micro-grooved PDMS surfaces with the mass ratio of base (DowsilTM 184 silicone elastomer base, Dow Europe GMHB C/O Dow Silicones Deutschland GMBH) to curing agent (DowsilTM 184 silicone elastomer curing agent, Dow Europe GMHB C/O Dow silicones Deutschland GMBH) fixed at 10:1 were fabricated using the peeling-off method.⁵² The groove width w of 20, 40, and 80 μm and groove height h of 10, 30, and 40 μm were set, respectively (the groove-to-groove spacing d was fixed at 20 μm). The mass ratio of the patterned surfaces was characterized using a laser scanning confocal microscopy (LSCM, ZEISS LSM900, Germany; laser wavelength: 405 nm), as shown in Fig. 1. Solid fraction $\phi = \frac{d}{w+d}$ and surface roughness $f = 1 + \frac{2h}{w+d}$ were used to characterize these surfaces.

TABLE I. Contact angles of water droplets on micro-grooved PDMS surfaces.

ϕ	f	θ_e		θ_a		θ_r	
		(L)	(T)	(L)	(T)	(L)	(T)
0.50	1.50	$125^\circ \pm 2^\circ$	$150^\circ \pm 2^\circ$	$137^\circ \pm 2^\circ$	$163^\circ \pm 2^\circ$	$111^\circ \pm 2^\circ$	$115^\circ \pm 2^\circ$
	2.50	$126^\circ \pm 2^\circ$	$147^\circ \pm 2^\circ$	$138^\circ \pm 2^\circ$	$164^\circ \pm 2^\circ$	$118^\circ \pm 2^\circ$	$118^\circ \pm 2^\circ$
	3.00	$125^\circ \pm 2^\circ$	$146^\circ \pm 2^\circ$	$133^\circ \pm 2^\circ$	$164^\circ \pm 2^\circ$	$110^\circ \pm 2^\circ$	$112^\circ \pm 2^\circ$
0.33	1.33	$136^\circ \pm 2^\circ$	$151^\circ \pm 2^\circ$	$142^\circ \pm 2^\circ$	$165^\circ \pm 2^\circ$	$122^\circ \pm 2^\circ$	$130^\circ \pm 2^\circ$
	2.00	$135^\circ \pm 2^\circ$	$146^\circ \pm 2^\circ$	$144^\circ \pm 2^\circ$	$165^\circ \pm 2^\circ$	$109^\circ \pm 2^\circ$	$113^\circ \pm 2^\circ$
	2.33	$125^\circ \pm 2^\circ$	$144^\circ \pm 2^\circ$	$144^\circ \pm 2^\circ$	$165^\circ \pm 2^\circ$	$118^\circ \pm 2^\circ$	$121^\circ \pm 2^\circ$
0.20	1.20	$140^\circ \pm 2^\circ$	$156^\circ \pm 2^\circ$	$155^\circ \pm 2^\circ$	$165^\circ \pm 2^\circ$	$132^\circ \pm 2^\circ$	$113^\circ \pm 2^\circ$
	1.60	$134^\circ \pm 2^\circ$	$143^\circ \pm 2^\circ$	$151^\circ \pm 2^\circ$	$167^\circ \pm 2^\circ$	$132^\circ \pm 2^\circ$	$125^\circ \pm 2^\circ$
	1.80	$128^\circ \pm 2^\circ$	$143^\circ \pm 2^\circ$	$148^\circ \pm 2^\circ$	$168^\circ \pm 2^\circ$	$127^\circ \pm 2^\circ$	$134^\circ \pm 2^\circ$

B. Measurement setup

Wettability of water droplets on these micro-grooved surfaces was measured using a droplet shape analyzer (DSA30, Krüss, Germany). The apparent contact angle for water droplets was measured from the profiles of water droplets with a nominal volume of $2.0 \mu\text{L}$. Contact angle hysteresis was obtained by tilting water droplets with volume ranging from 6.0 to $30.0 \mu\text{L}$ at the rotating speed of 30° per minute.^{53–55} When the droplets started moving downward, both advancing and receding contact angles were acquired from the distorted shapes. Considering the anisotropic wettability of these surfaces, all experiments were conducted at least three times from both longitudinal and transverse directions, which are denoted as “L” and “T,”

respectively. The ambient temperature and relative humidity for measuring surface wettability were $26 \pm 1^\circ\text{C}$ and $35\% \pm 2\%$, respectively.

Deionized water droplets with an initial radius r_0 in the range of 1.12 – 1.16 mm dropped freely from the height at the range from 1.11 to 211.78 mm with the help of a NE30 needle, and the impact process was recorded from both longitudinal and transverse directions using a high-speed camera (NAC HX-5E 75X, Japan) at $10\,000 \text{ fps}$. To elucidate the transition from CR to BDB, droplet impinging on the micro-grooved surface with a stripe height of $40 \mu\text{m}$ was recorded using a high-speed camera (NAC ACS-3, Japan) at $150\,000 \text{ fps}$ (though the transition from CR to SS was observed during the impact of droplets on the micro-grooved surface with a stripe height of $30 \mu\text{m}$, it is still difficult to observe the penetration of liquid into the cavities at $150\,000 \text{ fps}$). The

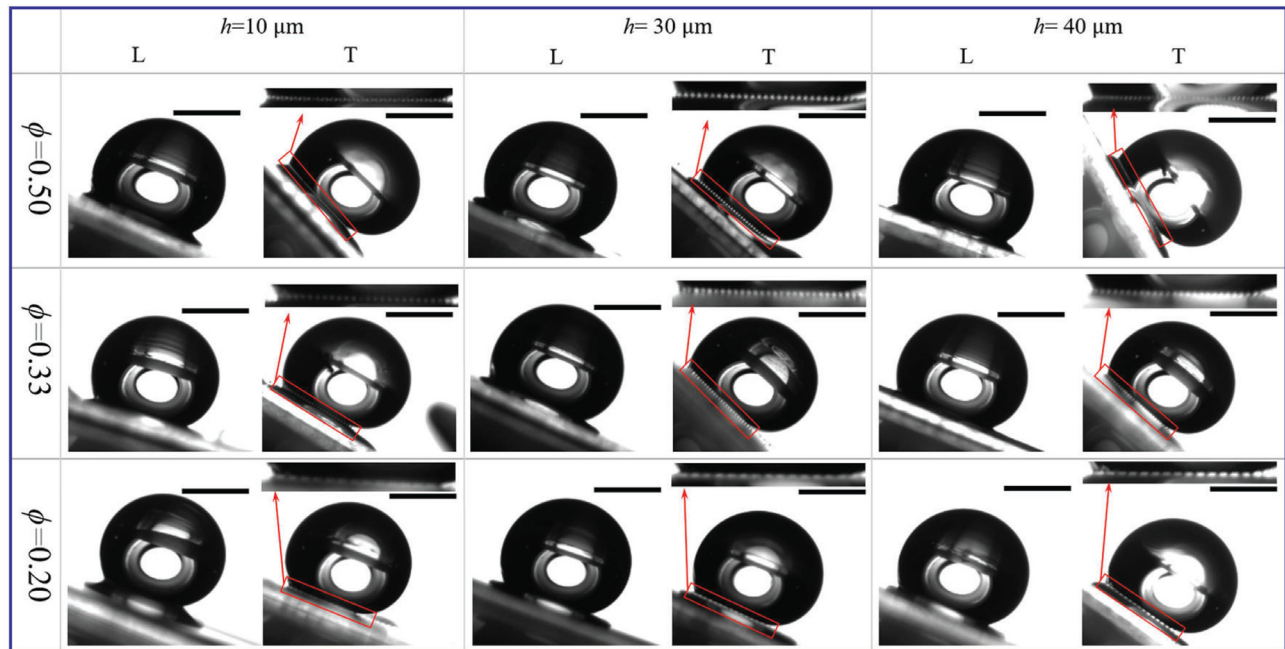


FIG. 2. Snapshots of water droplets starting moving downward on inclined micro-grooved PDMS surfaces. Scale bars all represent 1 mm .

ambient temperature and relative humidity for droplet impact experiments were $21 \pm 2^\circ\text{C}$ and $42\% \pm 4\%$, respectively. Each experiment was repeated at least four times to ensure the reproducibility. All videos were analyzed using the ImageJ software. The Weber number (We) defined as $We = \rho V_0^2 r_0 / \gamma_{lv}$ (where V_0 is the velocity of the center of an impinging droplet at the instant just before contacting the surfaces during the free fall, and ρ and γ_{lv} are water density and the liquid–vapor interfacial tension, respectively) was used for analysis.

III. RESULTS AND DISCUSSION

A. Wettability of micro-grooved PDMS surfaces

Table I lists the values of apparent (θ_e), advancing (θ_a), and receding (θ_r) contact angles for water droplets on these micro-grooved PDMS surfaces. θ_a and θ_r were determined from the snapshots of water droplets, which started moving downward on the inclined patterned surfaces, as shown in Fig. 2. It was found the static apparent, advancing, and receding contact angles have a corresponding larger value along the transverse direction than along the longitudinal direction, which is consistent with the observation by Zhao *et al.*⁵⁶ The reason is that when droplets advance or recede along the transverse direction, more energy barrier must be overcome.⁵⁶

B. Regime diagram of droplet impact

In this work, five impact phenomena were observed during the impact of de-ionized water droplets on micro-grooved PDMS surfaces depending on both impact velocity and surface roughness. When droplets fall from a relatively low location, they have not enough kinetic energy to overcome energy barrier due to contact angle hysteresis, and thus, they cannot bounce off the surfaces, which is called as NB (it is also called as deposition) [as shown in Fig. 3(a) (Multimedia view)]. Once the droplets have enough kinetic energy by increasing the falling height, they may bounce off the surface and such a phenomenon is called as CR [as shown in Fig. 3(b)]. Continuously increasing the impact velocity, the kinetic energy of the droplets becomes so large that part of the liquid penetrates into the cavities between micro-strips, resulting in more excess energy barrier due to the increase in adhesion between the liquid and the textured surface. Such an excess energy barrier prevents part of the liquid at the lowest place from leaving the surface, while other part of the liquid still departs from the surface. If there is only a minor part of liquid (no more than approximately 5% of the droplet) remaining on the surface, such a phenomenon is called as BDB [as shown in Fig. 3(c)]. PR is named for the case of a relatively larger volume of the liquid left on the surface [as shown in Fig. 3(d)]. In addition, SS was observed during droplet impinging on the patterned surfaces at a relatively high impact velocity [as shown in Fig. 3(e)] and its occurrence also depends on surface roughness, as shown in Fig. 4. Figures 4(a)–4(c) summarize regime diagrams of droplets impinging on these micro-grooved surfaces (the lower and upper limits of the Weber number for bouncing droplets, which are, respectively, denoted as We_{eL} and We_{eU} , are inserted as lines as shown in Fig. 4).

In addition, it should be noted that droplet oscillation during the free-falling of a water droplet and air friction is not considered in the above analyses. Droplet oscillation originates from its detachment from the NE30 needle, and such a phenomenon has

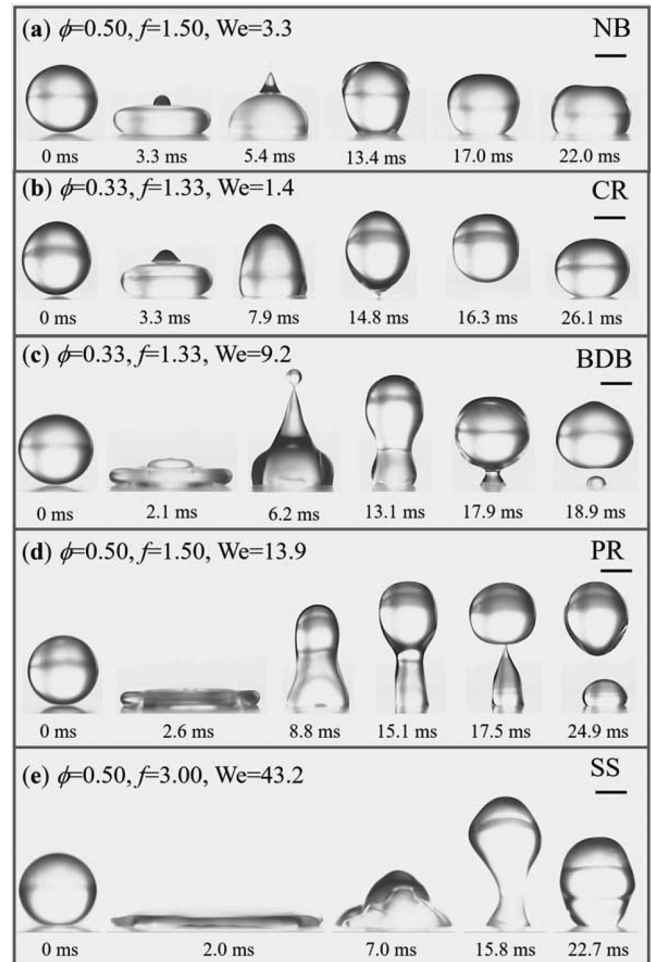


FIG. 3. Examples of droplet impact phenomenon. (a) NB, (b) CR, (c) BDB, (d) PR, and (e) SS. Scale bars all represent 1 mm. Multimedia views: <https://doi.org/10.1063/5.0134783.1>; <https://doi.org/10.1063/5.0134783.2>; <https://doi.org/10.1063/5.0134783.3>; <https://doi.org/10.1063/5.0134783.4>; <https://doi.org/10.1063/5.0134783.5>

been analyzed by Korshunov⁵⁷ (for more details, please see Ref. 57 and literature therein). During the free falling of a water droplet, it mainly experiences three forces, viz., gravity, buoyancy force, and air friction. Considering that the density of air is far less than that of water, the difference in the gravity and buoyancy force or the net gravity exerted on the droplet can be approximately expressed as $F_g = \frac{4}{3}\pi\rho g r_0^3$. The air friction force can be given as $F_d = 6\pi\eta r_0 v$ (Refs. 58 and 59), where η and v are the viscosity of air [20.2×10^{-6} Pa s (Refs. 59 and 60)] and falling speed of the droplet, respectively. For the case of a water droplet freely falling from a location at the height of about 220 mm, the falling speed when the location of the droplet is at 0 mm is about 2 m/s (maximum impact velocity). Taking these parameters, the net gravity and air friction force are calculated to be, respectively, $F_g = 62.4 \mu\text{N}$ and $F_d = 0.875 \mu\text{N}$, indicating that the effect of air friction force on the falling velocity of a spherical droplet can be neglected.

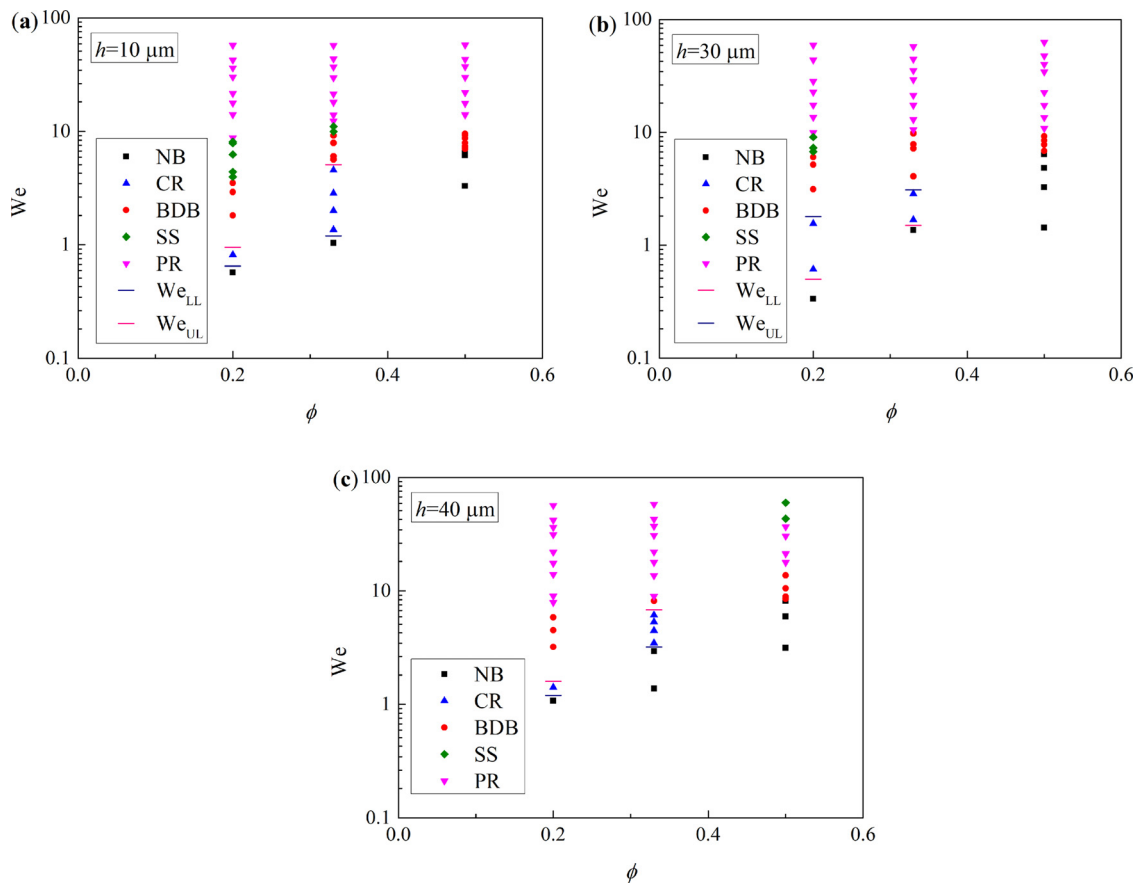


FIG. 4. Regime diagram for droplet impinging on micro-grooved PDMS surfaces with different stripe heights. (a) $h = 10$, (b) $h = 30$, and (c) $h = 40 \mu\text{m}$.

C. Prediction of the limits of impact velocity for bouncing droplets

In this part, both the lower and upper limits of impact velocity for bouncing droplets on micro-grooved surfaces were theoretically analyzed. For droplets bouncing off micro-pillared surfaces, the lower limit of impact velocity was obtained from the condition that the kinetic energy of the droplet just before contacting the surface $E_k = \frac{2}{3} \pi \rho V_0^2 r_0^3$ is equal to energy barrier due to contact angle hysteresis during the impact $E_s = \pi \gamma_{lv} r_{max}^2 (\cos \theta_r - \cos \theta_a)$ and expressed as⁴⁴

$$V_{CL} = \sqrt{\frac{3\gamma_{lv} r_{max}^2 (\cos \theta_r - \cos \theta_a)}{2\rho r_0^3}} \tag{1}$$

Considering the anisotropic wettability of micro-grooved surfaces, energy barrier due to contact angle hysteresis during the impact can be approximately expressed as⁴⁴

$$E_s = \pi \gamma_{lv} r_{max}^T r_{max}^L \sqrt{(\cos \theta_r^T - \cos \theta_a^T)(\cos \theta_r^L - \cos \theta_a^L)} \tag{2}$$

where r_{max}^T and r_{max}^L represent the maximum contact radii along the transverse and longitudinal directions, respectively. θ_a^T and θ_a^L represent the advancing contact angles measured from the transverse and

longitudinal directions, respectively. θ_r^T and θ_r^L represent the receding contact angles measured from the transverse and longitudinal directions, respectively. The values of θ_a^T , θ_a^L , θ_r^T , and θ_r^L are listed in Table I. Thus, by balancing E_k with E_s [Eq. (2)], the lower limit of impact velocity for bouncing droplets can be given as

$$V_{CL} = \sqrt{\frac{3\gamma_{lv} r_{max}^T r_{max}^L \sqrt{(\cos \theta_r^T - \cos \theta_a^T)(\cos \theta_r^L - \cos \theta_a^L)}}{2\rho r_0^3}} \tag{3}$$

As shown in Fig. 4, there exists a threshold of impact velocity to determine whether a phenomenon is classified as CR or BDB. This threshold is also named as the upper limit of impact velocity for bouncing droplets. As mentioned in Refs. 26, 27, 32, and 41–45, the existence of the upper impact velocity can be attributed to the wetting transition from the Cassie–Baxter state to the Wenzel state. To verify this hypothesis, water droplets impinging on micro-grooved PDMS surfaces were experimentally studied using a high-speed camera at 150 000 fps. Figure 5 shows the snapshots of some droplets impinging on the micro-grooved PDMS surface with $\phi = 0.20$ and $f = 1.80$. When We was very low ($We = 1.1$), it can be seen from the enlarged images that there was a visible gap between the liquid and the substrate

08 April 2024 03:53:22

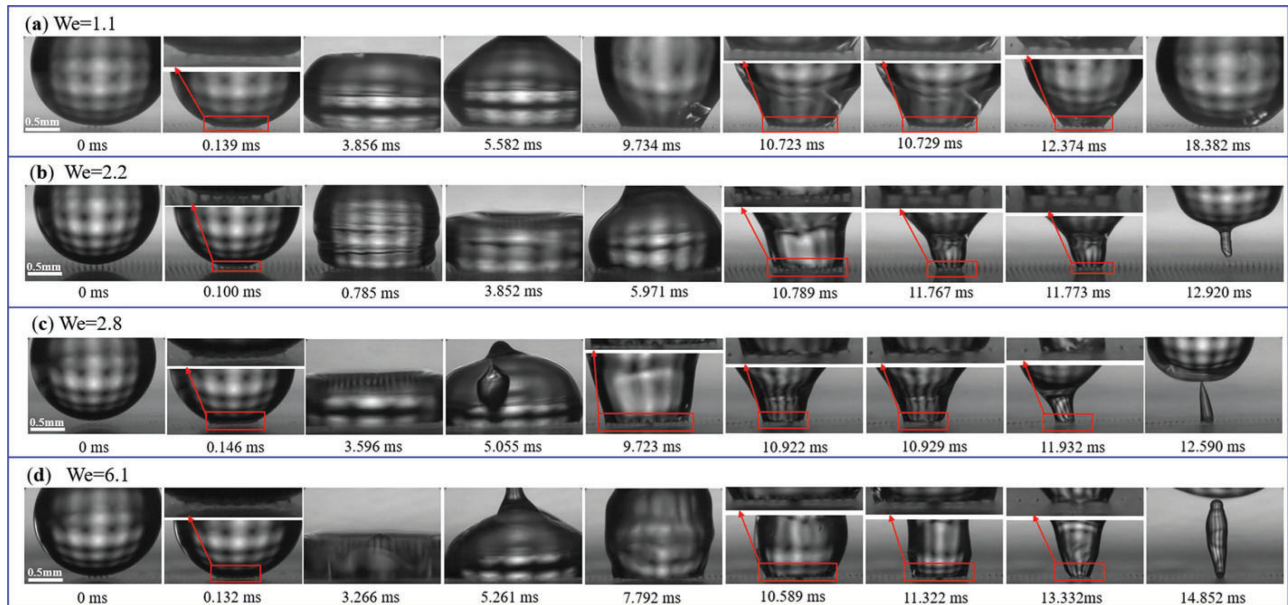


FIG. 5. Snapshots of droplets impinging on a micro-grooved PDMS surface with $\phi = 0.20$ and $f = 1.80$. Inserted scale bars represent 0.5 mm. Multimedia views: <https://doi.org/10.1063/5.0134783.6>; <https://doi.org/10.1063/5.0134783.7>; <https://doi.org/10.1063/5.0134783.8>; <https://doi.org/10.1063/5.0134783.9>

during the retraction process [as shown in Fig. 5(a) (Multimedia view)], indicating the droplet was currently at the Cassie–Baxter wetting state. Because the droplet did not have enough energy to overcome energy barrier due to contact angle hysteresis, the droplet could not bounce off the surface. When We was 2.2, visible gaps were also observed during the retraction process and the droplet completely bounced off the surface later [as shown in Fig. 5(b)] because it had enough kinetic energy to overcome energy barrier. When We was 2.8 [as shown in the enlarged images in Fig. 5(c)] or 6.1 [as shown in the enlarged images in Fig. 5(d)], one micro-groove was fully occupied with the liquid during the retraction process (a dark spot was observed between two neighbor micro-strips during the retraction process as shown in the enlarged images), indicating that there was a local wetting transition from the Cassie–Baxter state to the Wenzel state. Such a transition leads to a great increase in the adhesion between the liquid and the surface. As a result, the majority of the droplet departed from the surface with a minor part remaining on the surface, viz., a phenomenon of BDB was observed.

Figure 5 demonstrated that with the increase in impact velocity, more kinetic energy is available to force the penetration of liquid into the micro-grooves. When the liquid does not contact the bottom between the stripes, the droplets can still bounce off the surfaces. Based on our experimental observation and the works by Jung and Bhushan⁴⁵ and Wang *et al.*^{26,27} to predict the upper limit of impact velocity for droplets bouncing off micro-pillared surfaces, here a theoretical model was developed to predict the upper limit of impact velocity for droplets bouncing off micro-grooved surfaces, as shown in Fig. 6. Using the geometrical conditions $(\frac{w}{2})^2 + (r_1 - \delta)^2 = r_1^2$ and $\lambda^2 + (r_2 - \delta)^2 = r_2^2$ (where δ is the height of a meniscus between the microstrips, r_1 and r_2 are the two principal curvature radii, respectively), it is easy to obtain the relationships: $r_1 = \frac{w^2}{8\delta}$ and $r_2 = \frac{\lambda^2}{2\delta}$. Because the maximum of λ is several ten times greater than w , thus the Laplace pressure can be approximately expressed as

$$\Delta P = \gamma_{lv} \left(\frac{1}{r_1} + \frac{1}{r_2} \right) \approx \frac{8\gamma_{lv}\delta}{w^2}. \tag{4}$$

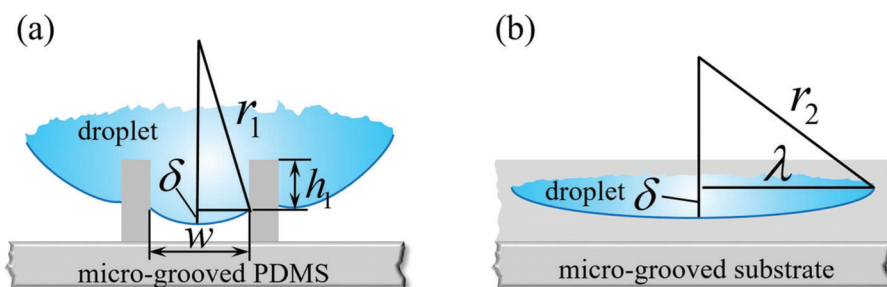


FIG. 6. Schematics for predicting the upper limit of impact velocity. (a) Along the transverse direction and (b) along the longitudinal direction.

TABLE II. Analysis for the lower and upper limits of impact velocity for bouncing droplets.

ϕ	f	r_{\max}^T (mm)	r_{\max}^L (mm)	V_{CL} (m/s)		V_{CU}^{exp} (m/s)	h_{1max} (μm)
				Exp.	Theor.		
0.50	1.50	1.79	1.98	0.67	0.29	0.67	9.84
	2.50	1.86	2.01	0.68	0.27	0.68	29.8
	3.00	1.94	2.13	0.76	0.32	0.76	39.8
0.33	1.33	1.32	1.62	0.21	0.19	0.62	9.46
	2.00	1.34	1.68	0.22	0.23	0.83	29.0
	2.33	1.60	1.82	0.24	0.25	0.73	39.3
0.20	1.20	1.26	1.43	0.18	0.19	0.37	9.24
	1.60	1.21	1.37	0.17	0.16	0.66	27.6
	1.80	1.28	1.56	0.21	0.17	0.46	38.8

In addition to the Laplace pressure, there are still dynamic pressure and water hammer pressure acting on impinging droplets. Because the action time of water hammer pressure is much shorter than the time of droplet impact, the effect on water

hammer pressure is not considered. The dynamic pressure can be given as⁴⁵

$$\Delta P_d = 0.5\rho V_0^2. \tag{5}$$

Balancing the Laplace pressure with the dynamic pressure, the upper limit of impact velocity (V_{CU}) for bouncing droplets can be given as

$$V_{CU} = \sqrt{\frac{16\gamma_{lv}\delta}{\rho w^2}}. \tag{6}$$

Using the critical geometric condition $h_{1max} + \delta = h$ (where h_1 is the penetration depth, as shown in Fig. 6), the upper limit of impact velocity can be further expressed as

$$V_{CU} = \sqrt{\frac{16\gamma_{lv}(h - h_{1max})}{\rho w^2}}. \tag{7}$$

The maximum of penetration depth can be given as

$$h_{1max} = h - \frac{\rho w^2 V_{CU}^2}{16\gamma_{lv}}. \tag{8}$$

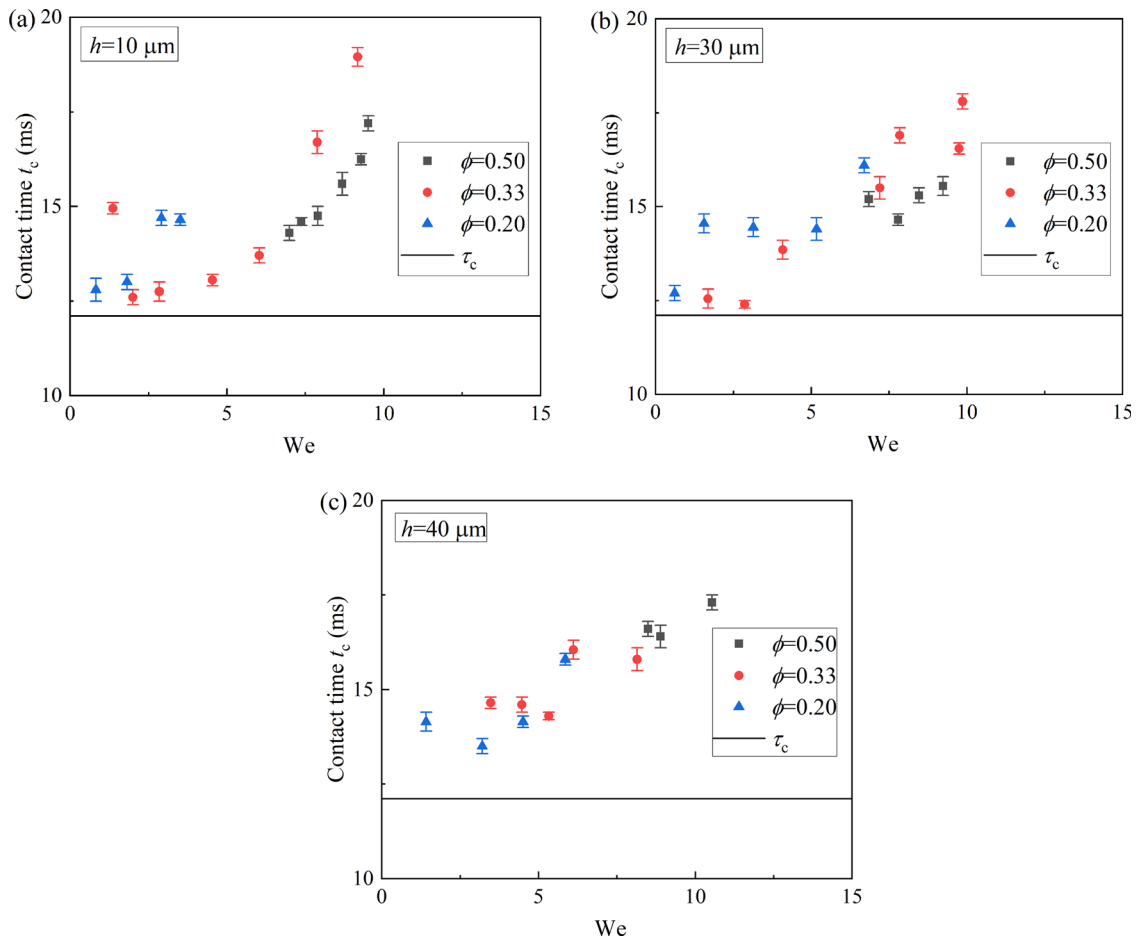


FIG. 7. Contact time of bouncing droplets on micro-grooved PDMS surfaces with different stripe heights. (a) $h = 10$, (b) $h = 30$, and (c) $h = 40 \mu\text{m}$.

Table II lists the analysis for the lower and upper limits of impact velocity for bouncing droplets. The theoretical values of the lower limit of impact velocity were all underestimated, which could be attributed to the neglect of energy dissipation and the underestimation of the liquid–vapor interfacial area. Substituting the experimental values of the upper impact velocity for each case and other parameters into Eq. (8), the maximum of penetration depth h_1 was obtained and listed in Table II, indicating that at the critical point, one or more micro-grooves were nearly occupied with the liquid.

D. Contact time of bouncing droplets

The contact time is an important parameter for impinging droplets. As mentioned in Refs. 26 and 47–50, the contact time can be reduced to a great extent by designing micro-/nano-patterned surfaces. The characteristic value of the contact time τ is $2.6\sqrt{\rho r_0^3/\gamma_{lv}}$ (Ref. 47). Figure 7 shows the contact time of impinging droplets on the micro-grooved PDMS surfaces in our experiments (although a minor quantity of liquid was left on the surfaces for the case of BDB, the contact time for this case was also included). From Fig. 7, it can be found that the values of the contact time were all larger than the characteristic value, which could be attributed to the anisotropic wettability of micro-grooved surfaces. Moreover, with the decrease in the Weber number, there was usually a shorter contact time, which could be attributed to the penetration of liquid. More liquid penetration induces the increase in the actual solid–liquid interfacial area, which will hinder the retraction of droplets more greatly (Table III). We also found that for the case of droplets impinging on a micro-grooved surface with a solid fraction of 0.50 and surface roughness of 1.33, the contact time for We of 1.4 was longer than that for We of 4.5, which might be attributed to the small extent of liquid penetration because the values of impact velocity for the two cases are both relatively low. In conclusion, surface roughness only had a small influence on reducing the contact time.

The contact time (t_c) can be divided into three parts, viz., spreading time (t_s), time of the pinned contact line stage (t_p), and retraction time (t_R). Considering the anisotropic wetting characteristics of micro-grooved surfaces, t_s , t_p , and t_R all had different values along the longitudinal and transverse directions, as shown in Table III. From Table III, it can be seen that bouncing droplets all had a relatively a longer spreading time, a shorter time for the contact line pinning stage, and a relatively longer retraction time along the longitudinal direction than along the transverse direction, which could be attributed to the fact that the liquid spreads more easily along the longitudinal direction than along the transverse direction.

IV. CONCLUSIONS

Water droplets impinging on micro-grooved PDMS surfaces were experimentally studied. Different phenomena including NB, CR, BDD, PR, and SS were observed depending on impact velocity and surface roughness. The transition from CR to BDB was further studied experimentally, and it was found that this transition can be attributed to the local wetting transition from the Cassie–Baxter state to the Wenzel state. Both the lower and upper limits of impact velocity for bouncing droplets were theoretically analyzed. In addition, the contact time of bouncing droplets was also discussed. It was found that there was a shorter contact time with the decrease in Weber number and surface roughness only had a small influence on the contact time. We envision that this work will highlight the application of droplets and

TABLE III. Analysis of contact time of bouncing droplets (unit: ms).

ϕ	f	We	t_c	t_s^L	t_s^T	t_p^L	t_p^T	t_R^L	t_R^T	Note		
0.50	1.50	7.0	14.4	2.5	2.2	1.9	3.0	10.0	9.2	BDB		
		8.7	15.7	2.3	2.1	1.5	3.3	11.9	10.3	BDB		
		9.5	17.3	2.4	2.1	1.7	3.3	13.2	11.9	BDB		
	2.50	6.8	15.2	2.8	2.5	1.1	2.7	11.3	10.0	BDB		
		9.3	15.6	2.5	2.4	0.9	1.7	12.2	11.5	BDB		
		8.5	16.7	2.6	2.4	1.7	2.8	12.4	11.5	BDB		
	3.00	10.5	17.2	2.4	2.1	1.9	3.4	12.9	11.7	BDB		
		0.33	1.33	1.4	14.9	3.4	3.2	2.9	4.6	8.6	7.1	CR
			4.5	13.0	2.4	2.5	2.2	3.5	8.4	7.0	CR	
6.0	13.8		2.1	2.2	1.6	3.0	10.1	8.6	BDB			
2.00	9.2	19.1	2.4	2.1	1.2	2.3	15.5	14.7	BDB			
	1.7	12.4	3.0	3.0	2.2	4.3	7.2	5.1	CR			
	7.2	15.5	2.4	2.3	0.9	2.4	12.2	10.8	CR			
2.33	8.1	16.9	2.4	2.2	1.1	2.4	13.4	12.3	BDB			
	3.5	14.7	2.8	2.8	1.8	4.0	10.1	7.9	CR			
	6.1	15.8	2.6	2.3	1.5	3.7	11.7	9.8	CR			
0.20	1.20	8.1	15.9	2.4	2.2	1.7	2.7	11.8	11.0	BDB		
		0.8	12.8	3.8	3.2	2.2	4.8	6.8	4.8	CR		
		1.8	12.9	3.8	3.2	2.3	4.8	6.8	4.9	BDB		
1.60	3.5	14.7	2.3	2.6	1.8	4.1	10.6	8.0	BDB			
	0.6	12.8	3.4	3.9	1.4	3.7	8.0	5.2	CR			
	1.6	14.6	3.0	2.9	1.0	4.1	10.6	7.6	CR			
1.80	3.1	14.3	2.8	2.8	1.2	2.4	10.3	9.1	BDB			
	6.7	16.0	2.1	2.3	1.7	2.2	12.2	11.5	BDB			
	1.4	14.1	3.9	4.0	1.9	4.0	8.3	6.1	CR			
5.9	3.2	13.6	3.1	2.4	1.8	4.0	8.7	7.2	BDB			
	15.8	2.7	2.6	1.1	2.2	12.0	11.0	BDB				

patterned surfaces with anisotropic wetting characteristics in agricultural and industrial fields.

ACKNOWLEDGMENTS

This work was jointly supported by the National Natural Science Foundation of China (Grant Nos. 11572114 and 12272085), the PetroChina Innovation Foundation (Grant No. 2019D-5007-0102), the Chinese Academy of Sciences Key Research Program of Frontier Sciences (Grant No. QYZDJ-SSW-JSC019), and the Innovation Demonstration Base of Ecological Environment Geotechnical and Ecological Restoration of Rivers and Lakes (Grant No. 2020EJB004).

AUTHOR DECLARATIONS

Conflict of Interest

The authors have no conflicts to disclose.

Author Contributions

Shizheng Wang: Conceptualization (equal); Data curation (lead); Investigation (lead); Methodology (equal); Writing – original draft (lead).

Xianfu Huang: Conceptualization (equal); Funding acquisition (equal); Methodology (equal); Writing – review & editing (equal). **Longquan Chen:** Conceptualization (equal); Funding acquisition (equal); Writing – review & editing (equal). **Ying-Song Yu:** Conceptualization (equal); Data curation (equal); Funding acquisition (lead); Methodology (equal); Supervision (lead); Writing – review & editing (lead).

DATA AVAILABILITY

The data supporting the findings of this study are available from the corresponding authors upon reasonable request.

REFERENCES

- ¹D. Y. Xia, L. M. Johnson, and G. P. López, “Anisotropic wetting surfaces with one-dimensional and directional structures: Fabrication approaches, wetting properties and potential applications,” *Adv. Mater.* **24**(10), 1287–1302 (2012).
- ²Y. F. Zhong, A. M. Jacobi, and J. G. Georgiadis, “Effect of surface chemistry and groove geometry on wetting characteristics and droplet motion of water condensate on surfaces with rectangular microgrooves,” *Int. J. Heat Mass Transfer* **57**(2), 629–641 (2013).
- ³P. Goel, S. Kumar, R. Kapoor, and J. P. Singh, “Mechanical strain induced wetting transitions between anisotropic and isotropic on polydimethylsiloxane (PDMS) films patterned by optical discs,” *Appl. Surf. Sci.* **356**, 102–109 (2015).
- ⁴T. Pratap and K. Patra, “Direction dependent dynamic wetting of semi-hemispherical end micro-groove textured Ti-6Al-4V surface,” *Surf. Coating Technol.* **356**, 138–149 (2018).
- ⁵M. Kumar, R. Bhardwaj, and K. C. Sahu, “Motion of a droplet on an anisotropic microgrooved surface,” *Langmuir* **35**(8), 2957–2965 (2019).
- ⁶Y. L. Xiang, S. L. Huang, T. Y. Huang, A. Dong, D. Cao, H. Y. Li, Y. H. Xue, P. Y. Lv, and H. L. Duan, “Superrepellency of underwater hierarchical structures on *Salvinia* leaf,” *Proc. Natl. Acad. Sci. U. S. A.* **117**(5), 2282–2287 (2020).
- ⁷H. Wang, M. He, H. Liu, and Y. Guan, “Controllable water behaviors on V-shape micro-grooved titanium alloy surfaces depending on the depth-to-width aspect ratio,” *Mater. Today Phys.* **20**, 100461 (2021).
- ⁸Q. Peng, L. Jia, Y. Ding, C. Dang, L. F. Yin, and X. Yan, “Influence of groove orientation on dropwise condensation on hydrophobic and hierarchical superhydrophobic surfaces with microgroove arrays,” *Int. Commun. Heat Mass Transfer* **112**, 104492 (2020).
- ⁹C. Jossierand and S. T. Thoroddsen, “Drop impact on a solid surface,” *Annu. Rev. Fluid Mech.* **48**(1), 365–391 (2016).
- ¹⁰D. Khojasteh, M. Kazerooni, S. Salarian, and R. Kamali, “Droplet impact on superhydrophobic surfaces: A review of recent developments,” *J. Ind. Eng. Chem.* **42**, 1–14 (2016).
- ¹¹R. N. Wenzel, “Resistance of solid surfaces to wetting by water,” *Ind. Eng. Chem.* **28**(8), 988–994 (1936).
- ¹²A. B. D. Cassie and S. Baxter, “Wettability of porous surfaces,” *Trans. Faraday Soc.* **40**, 546–551 (1944).
- ¹³Q. S. Zheng, Y. Yu, and Z. H. Zhao, “Effects of hydraulic pressure on the stability and transition of wetting modes of superhydrophobic surfaces,” *Langmuir* **21**(26), 12207 (2005).
- ¹⁴A. Tuteja, W. Choi, M. L. Ma, J. M. Mabry, S. A. Mazzella, G. C. Rutledge, G. H. McKinley, and R. E. Cohen, “Designing superoleophobic surfaces,” *Science* **318**(5856), 1618–1622 (2007).
- ¹⁵A. Marmur, “Wetting on hydrophobic rough surfaces: To be heterogeneous or not to be?” *Langmuir* **19**(20), 8343–8348 (2003).
- ¹⁶A. Lafuma and D. Quéré, “Superhydrophobic states,” *Nat. Mater.* **2**(7), 457–460 (2003).
- ¹⁷J. Bico, C. Marzolin, and D. Quéré, “Pearl drops,” *Europhys. Lett.* **47**(2), 220–226 (1999).
- ¹⁸J. Lou, S. L. Shi, C. Ma, C. J. Lv, and Q. S. Zheng, “Suspended penetration wetting state of droplets on microstructured surfaces,” *Sci. China: Phys. Mech. Astron.* **64**, 244711 (2021).
- ¹⁹E. Bormashenko, R. Pogreb, G. Whyman, Y. Bormashenko, and M. Erlich, “Vibration-induced Cassie-Wenzel transition on rough surfaces,” *Appl. Phys. Lett.* **90**(20), 201917 (2007).
- ²⁰A. Sudeepthi, L. Yeo, and A. K. Sen, “Cassie-Wenzel wetting transition on nanostructured superhydrophobic surfaces induced by surface acoustic waves,” *Appl. Phys. Lett.* **116**(9), 093704 (2020).
- ²¹P. C. Tsai, R. G. H. Lammertink, M. Wessling, and D. Lohse, “Evaporation-triggered wetting transition for water droplets upon hydrophobic microstructures,” *Phys. Rev. Lett.* **104**(11), 116102 (2010).
- ²²R. Chen, L. Jiao, X. Zhu, Q. Liao, D. D. Ye, B. Zhang, W. Li, Y. P. Lei, and D. L. Li, “Cassie-to-Wenzel transition of droplet on the superhydrophobic surface caused by light induced evaporation,” *Appl. Therm. Eng.* **144**, 945–959 (2018).
- ²³C. Luo, M. M. Xiang, X. C. Liu, and H. Wang, “Transition from Cassie-Baxter to Wenzel states on microline-formed PDMS surfaces induced by evaporation or pressing of water droplets,” *Microfluid. Nanofluid.* **10**(4), 831–842 (2011).
- ²⁴G. H. Li, X. Y. Yang, X. F. Huang, and Y. S. Yu, “Wettability and evaporation of dilute sodium dodecyl sulfate droplets on micropillar-arrayed non-wetting surfaces,” *Int. J. Heat Mass Transfer* **194**(8), 123058 (2022).
- ²⁵Y. Liu, L. Moevius, X. Xu, T. Qian, J. M. Yeomans, and Z. Wang, “Pancake bouncing on superhydrophobic surfaces,” *Nat. Phys.* **10**(7), 515–519 (2014).
- ²⁶L. Z. Wang, A. Zhou, J. Z. Zhou, L. Q. Chen, and Y. S. Yu, “Droplet impact on pillar-arrayed non-wetting surfaces,” *Soft Matter* **17**(24), 5932–5940 (2021).
- ²⁷L. Z. Wang, X. F. Huang, Q. Z. Yuan, L. Q. Chen, and Y. S. Yu, “Dilute sodium dodecyl sulfate droplets impact on micropillar-arrayed non-wetting surfaces,” *Phys. Fluids* **33**(10), 107103 (2021).
- ²⁸N. D. Patil, R. Bhardwaj, and A. Sharma, “Droplet impact dynamics on micropillar hydrophobic surfaces,” *Exp. Therm. Fluid Sci.* **74**, 195–206 (2016).
- ²⁹M. Broom and G. R. Willmott, “Water drop impacts on regular micropillar arrays: The impact region,” *Phys. Fluids* **34**, 017115 (2022).
- ³⁰C. J. Lv, P. F. Hao, X. W. Zhang, and F. He, “Drop impact upon superhydrophobic surfaces with regular and hierarchical roughness,” *Appl. Phys. Lett.* **108**(14), 141602 (2016).
- ³¹Z. M. Chu, W. C. Jiao, X. F. Huang, L. Y. Chen, Y. T. Zheng, R. G. Wang, and X. D. He, “Directional rebound control of droplets on low-temperature regular and irregular wrinkled superhydrophobic surfaces,” *Appl. Surf. Sci.* **530**, 147099 (2020).
- ³²L. K. Malla, N. D. Patil, R. Bhardwaj, and A. Neild, “Droplet bouncing and breakup during impact on a microgrooved surface,” *Langmuir* **33**(38), 9620–9631 (2017).
- ³³D. Song, B. W. Song, H. B. Hu, X. S. Du, and Z. B. Ma, “Contact angle and impinging process of droplets on partially grooved hydrophobic surfaces,” *Appl. Therm. Eng.* **85**, 356–364 (2015).
- ³⁴V. Fink, A. Stroh, R. Bernard, J. Kriegseis, B. Frohnappel, H. Marshall, and M. Wörner, “Drop bouncing by micro-grooves,” *Int. J. Heat Fluid Flow* **70**, 271–278 (2018).
- ³⁵Y. L. Fan, Z. B. Zhan, C. L. Guo, J. H. Kim, and J. K. Lee, “Retraction dynamics of a water droplet impacting onto a microgrooved hydrophobic surface at different velocities and surface temperatures,” *Int. J. Heat Mass Transfer* **168**, 120851 (2021).
- ³⁶Y. X. Wang, M. P. Jian, and X. W. Zhang, “Lateral motion of a droplet after impacting on groove-patterned superhydrophobic surfaces,” *Colloid Surf. A* **570**, 48–54 (2019).
- ³⁷C. Liu, I. Legchenkova, L. B. Han, W. N. Ge, C. J. Lv, S. L. Feng, E. Bormashenko, and Y. H. Liu, “Directional droplet transport mediated by circular groove arrays,” *Langmuir* **36**(32), 9608–9615 (2020).
- ³⁸C. Liu, I. Legchenkova, L. B. Han, W. N. Ge, C. J. Lv, S. L. Feng, E. Bormashenko, and Y. H. Liu, “Directional droplet transport mediated by circular groove arrays—Part II: Theory of effect,” *Langmuir* **37**(5), 1948–1953 (2021).
- ³⁹D. Kwon, S. Lee, and E. Yeom, “Experimental investigation on water repellency and anisotropic wettability of microgrooved polymer surfaces,” *Exp. Fluids* **60**(11), 169 (2019).
- ⁴⁰C. F. Guo, L. Liu, J. X. Sun, C. W. Liu, and S. Y. Liu, “Splashing behavior of impacting droplets on grooved superhydrophobic surfaces,” *Phys. Fluids* **34**, 052105 (2022).

- ⁴¹M. Abolghasemibizaki and R. Mohammadi, “Droplet impact on superhydrophobic surfaces fully decorated with cylindrical macrotextures,” *J. Colloid Interface Sci.* **509**, 422–431 (2018).
- ⁴²C. Lee, Y. Nam, H. Lastakowski, D. I. Hur, S. Shin, A. L. Biance, C. Pirat, C. J. Kim, and C. Ybert, “Two types of Cassie-to-Wenzel wetting transitions on superhydrophobic surfaces during drop impact,” *Soft Matter* **11**(23), 4592–4599 (2015).
- ⁴³D. Bartolo, F. Bouamrine, É. Verneuil, A. Buguin, P. Silberzan, and S. Moulinet, “Bouncing or sticky droplets: Impalement transitions on superhydrophobic micropatterned surfaces,” *Europhys. Lett.* **74**(2), 299–305 (2006).
- ⁴⁴M. Reyssat, A. Pépin, F. Marty, Y. Chen, and D. Quéré, “Bouncing transitions on microtextured materials,” *Europhys. Lett.* **74**(2), 306–312 (2006).
- ⁴⁵Y. C. Jung and B. Bhushan, “Dynamic effects of bouncing water droplets on superhydrophobic surfaces,” *Langmuir* **24**(12), 6262–6269 (2008).
- ⁴⁶S. L. Shi, C. J. Lv, and Q. S. Zheng, “Drop impact on two-tier monostable superrepellent surfaces,” *ACS Appl. Mater. Interfaces* **11**(46), 43698–43707 (2019).
- ⁴⁷D. Richard, C. Clanet, and D. Quéré, “Contact time of a bouncing drop,” *Nature* **417**(6891), 811 (2002).
- ⁴⁸J. C. Bird, R. Dhiman, H. M. Kwon, and K. K. Varanasi, “Reducing the contact time of a bouncing drop,” *Nature* **503**(7476), 385–388 (2013).
- ⁴⁹S. R. Gao, B. J. Wei, J. X. Jin, J. S. Ye, Y. F. Wang, S. F. Zheng, Y. R. Yang, and X. D. Wang, “Contact time of a droplet impacting hydrophobic surfaces,” *Phys. Fluids* **34**, 067104 (2022).
- ⁵⁰J. Y. Du, X. Wang, Y. Z. Li, and Q. Min, “Surface design of superhydrophobic parallel grooves for controllable petal bouncing and contact time reduction,” *Phys. Fluids* **34**, 082105 (2022).
- ⁵¹F. C. Wang, J. T. Feng, and Y. P. Zhao, “The head-on colliding process of binary liquid droplets at low velocity-high-speed photography experiments and modeling,” *J. Colloid Interface Sci.* **326**, 196–200 (2008).
- ⁵²Y. S. Yu, X. F. Huang, L. Sun, J. Z. Zhou, and A. Zhou, “Evaporation of ethanol/water mixture droplets on micro-patterned PDMS surfaces,” *Int. J. Heat Mass Transfer* **144**, 118708 (2019).
- ⁵³A. Carre and M. E. R. Shanahan, “Drop motion on an inclined plane and evaluation of hydrophobic treatments to glass,” *J. Adhes.* **49**(3–4), 177–185 (1995).
- ⁵⁴A. Nakajima, T. Miyamoto, M. Sakai, T. Isobe, and S. Matsushita, “Comparative study of the impact and sliding behavior of water droplets on two different hydrophobic silane coatings,” *Appl. Surf. Sci.* **292**, 990–996 (2014).
- ⁵⁵Y. Wang, M. Jian, H. Liu, and X. Zhang, “Anisotropic wetting of droplets on stripe-patterned chemically heterogeneous surfaces: Effect of length ratio and deposition position,” *Langmuir* **35**(12), 4387–4396 (2019).
- ⁵⁶Y. Zhao, Q. Lu, M. Li, and X. Li, “Anisotropic wetting characteristics on submicrometer-scale periodic grooved surface,” *Langmuir* **23**(11), 6212–6217 (2007).
- ⁵⁷A. I. Korshunov, “Oscillations of a water droplet separated from the connection,” *Fluid Dyn.* **50**(4), 585–589 (2015).
- ⁵⁸L. Prandtl, *Essentials of Fluid Dynamics* (Hafner Publishing Company, New York, 1952), p. 106.
- ⁵⁹L. D. Landau and E. M. Lifshitz, *Fluid Mechanics*, 2nd ed. (Pergamon Press, Beijing, 1987), pp. 46–61.
- ⁶⁰H. Tomlinson, “The coefficient of viscosity of air,” *Philos. Trans. R. Soc. London* **177**, 767–799 (1886).